Journal of the Brazilian Society of Mechanical Sciences and Engineering (2023) 45:291
https://doi.org/10.1007/s40430-023-04180-3

TECHNICAL PAPER

Crashworthiness evaluation of hybrid tubes made of GFRP composite and aluminum tubes filled with honeycomb structures

Sinem K. Mert[1] · Mehmet Ali Güler[2] · Murat Altin[3] · Erdem Acar[4] · Adem Çiçek[1]

Received: 9 January 2023 / Accepted: 16 March 2023 / Published online: 6 May 2023

Abstract

Metal/composite hybrid tubes are potential candidates for crashworthy products having less weight and low cost compared to conventional crash boxes. The crashworthiness of Al/GFRP tubes created by wrapping an aluminum 6082 tube in glass fiber-reinforced plastic is the subject of this investigation. To compare the crush behavior of the empty GFRP/hybrid and honeycomb-filled hybrid circular tubes, quasi-static tests were conducted. Bundles and cracks were observed during the tests of composite and hybrid tubes. Energy absorption parameters of the numerical model were compared with the results of experiments. The crushing behavior of the GFRP and hybrid specimens was simulated using a numerical approach based on the Chang–Chang damage criteria. It is found that trigger mechanisms performed in the FE analysis can effectively model the crashing behavior of GFRP/hybrid specimens. The CFE and SEA of the empty composite tube are 95% and 29% greater than the empty hybrid tube, respectively. The effect of honeycomb filling on the energy absorption capabilities of hybrid tubes is investigated. The CFE of the honeycomb-filled hybrid tube is found to be 4.5% greater than the CFE of the empty hybrid tube.

Keywords Crashworthiness · Energy absorption · Al/GFRP hybrid tube · Honeycomb filling

1 Introduction

Various passive safety structures are employed in the design of automobile structures to prevent the fatal injuries of drivers and passengers in the case of a crash. In this respect, thin-walled tubes are generally used since they dissipate the kinetic energy by progressive deformation and minimize the damage to the fundamental parts of the vehicle. Several studies were conducted to optimize the energy absorption capacity of tubular sections by employing different materials for tubular structures, such as steel [1–3], aluminum [4–10], kevlar fiber [11], kenaf fiber [12, 13], aramid fiber [14], glass fiber [15] and carbon fiber [14, 16–19].

Composite energy absorbers differ mechanically from their metallic counterparts in a variety of ways. Higher strength, lighter weight, higher specific stiffness, and better potential for vibration and noise reduction are some of these features. Composite tubular structures exhibit better crashworthiness performance through progressive crushing by a combination of several mechanisms involving fiber/matrix fracture, splitting, and delamination [20]. Circular, square, and cone composite crash tubes were used in automotive applications to absorb more energy while deforming progressively or catastrophically.

Technical Editor: João Marciano Laredo dos Reis.

✉ Mehmet Ali Güler
mehmet.guler@aum.edu.kw

Sinem K. Mert
sinemkocaoglanmert@gmail.com

Murat Altin
maltin@gazi.edu.tr

Erdem Acar
acar@etu.edu.tr

Adem Çiçek
acicek@ybu.edu.tr

[1] Department of Mechanical Engineering, Ankara Yildirim Beyazit University, Ankara 06010, Turkey

[2] College of Engineering and Technology, American University of the Middle East, Egaila 54200, Kuwait

[3] Department of Automotive Engineering, Gazi University, Ankara, Turkey

[4] Department of Mechanical Engineering, TOBB University of Economics and Technology, Ankara 06560, Turkey

The higher material cost of carbon fibers, which appears to limit their wide range of use, is in contrast to their superior mechanical performance and lightweight features. Compared to carbon and other fibers, glass fiber has a lower material cost, which has generated a lot of interest in its use in energy absorbing structures [20, 21]. Effects of various parameters on crashworthiness performance of glass fiber-reinforced polymer (GFRP) tubes have been investigated by many researchers. Ozbek et al. [15] investigated lateral crushing glass-carbon intraply fiber-reinforced tubes. Wang et al. [22] evaluated the impact of temperature on the crashworthiness of GFRP tubes with circular cross sections and foam fillers inside. They found that the temperature increase led to a reduction in the crashworthiness ability. They also concluded that using the foam with [0/90] fiber orientation angle and higher density for the GFRP structure improved the tube's crush force efficiency. Palanivelu et al. [23] evaluated the effects of geometry and trigger type on the energy absorption characteristics of uni-directional GFRP tubes produced by hand-laying up resin with single and double plies. The tubes having a 45° chamfer trigger resulted in a higher peak force compared to the tubes with a tulip trigger. They showed that circular tubes have better crashworthiness performance compared to square and hexagonal-shaped tubes. Later, Ozbek et al. [24] studied circular cut-outs to create a trigger mechanism in glass/epoxy composite tubes that were subjected to quasi-static axial compression loads. The design criteria for the trigger mechanism under investigation took into account the quantity, distribution, and size of the circular cut-outs. They found that the increase in the diameter of the cut-outs led to an increase in efficiency and a reduction in peak load. Chen et al. [25] investigated carbon fiber reinforced polymer (CFRP), GFRP, and CFRP/GFRP inter-layer hybridized composite tubes with a single 45° chamfer trigger (T1), a combined 45° chamfer and outward-folding crush-cap (T2), and a combined 45° chamfer and outward-folding crush-cap with a cavity (T3). For the tube with the T2 trigger mechanism, the initial peak crushing force was reduced by 35.5% in the GFRP composite tube compared to the CFRP composite tube, and the mean crush force (MCF) and specific energy absorption (SEA) were increased by 68.6% and 98.5%, respectively. Awdallah et al. [26] studied the crashworthiness performance of GFRP square tubes with cutouts. Their results showed that the hole diameter impacted the SEA values the most. Moreover, they concluded that the GFRP tubes with circular cuts performed 22.05 and 61.16% higher for SEA and CFE than the complete specimens.

Researchers also investigated the effect of foam filling on the crashworthiness ability of GFRP tubes. Wang et al. [27], Othman et al. [28], and Chen et al. [29] examined the enhancement of the crashworthiness behavior of composite tubes by using polyurethane (PU) foam filler. Wang et al. [27] found that PU foam-filled GFRP tubes absorb more energy than foam-filled Al tubes. However, the peak load was not affected by the density of the foam. Moreover, tubes with $[0/90]$ fiber orientation had higher peak force than tubes with $[\pm 45]$ fiber orientation. Othman et al. [28] tested square tubes made of E-glass under axial and oblique loading conditions. Experimental results indicated that the tube with PU foam filler performed better crashworthiness performance than the empty composite tube. Also, they observed a decrease in the mean force and absorbed energy when the angle of the oblique load increased. Jin et al. [30] proposed lattice frame reinforcement for the GFRP tube with foam filler inside. They found that lattice frame and syntactic foam enhanced energy absorption by 90%. Wang et al. [31] tested an epoxy resin syntactic foam core filled GFRP tube, which has a multi-cell geometry. They showed that energy absorption increased by 48% when the number of webs of GFRP tubes was increased from 0 to 4. Sarkhosh et al. [32] experimentally investigated the crashworthiness characteristics of cylindrical hollow composite tubes, tubes filled with aluminum honeycomb, tubes filled with polyurethane foam, and tubes filled with a combination of polyurethane foam and aluminum honeycomb. Foam and honeycomb fillers worked together as a trigger and prevented the tube from failing catastrophically during the crushing process. The mean forces of the tubes filled with both polyurethane foam and aluminum honeycomb increased up to 33% compared to hollow tubes, making them the best tubes in their study in terms of the mean force and the total energy absorption.

The advantages of hybrid tubes were investigated experimentally in terms of cost and crashworthiness performance. Jiang et al. [33] studied failure mechanisms of carbon-glass-kevlar hybrid fiber reinforced polymer (HFRP) composites to examine hybridization effects. Compared to carbon and kevlar tubes, it is discovered that HFRP has 152.9% and 76.2% higher energy absorption. Mirzaei et al. [34] and Song et al. [35] examined circular metal tubes wrapped with glass/epoxy composite to produce hybrid tubes. Mirzaei et al. [34] explored the influences of orientation on the deformation mechanism of aluminum/GFRP tubular sections. Contrary to previously reported results, which found that the best fiber orientation is the hoop direction, they found that hybrid tubes with multi angle ply patterns can have better crashworthiness behavior. They also proposed an analytical model which successfully predicts the mean force and folding length. Song et al. [35] studied the crashworthiness behavior of circular metal tubes wrapped with glass/epoxy under dynamic loading. The specimens were fabricated with $[\pm 15]_3$, $[\pm 45]_3$, and $[\pm 90]_6$ orientation by winding-up process to examine the impacts of the ply orientation. The best energy absorption efficiency was obtained for the tubes with $[\pm 90]_6$ orientation. Shin et al. [36] tested aluminum tubes wrapped GFRP around with [0], [90], [0/90], and

[±45] orientations under quasi-static conditions. The tube with a [90] ply orientation absorbed the highest energy. The hybrid tubes had a larger mean force and absorbed more energy in comparison to the aluminum tubes. Tarafdar et al. [37] evaluated the performance of hybrid sandwich tubes with multi-cell geometry and hierarchical cores inside. They compared hybrid tubes consisting of Al and GFRP tubes under quasi-static loading. In Al tubes, the load declines after the peak force is observed and fluctuate at a lower mean force compared to GFRP tubes. The composite tube performed higher crush force efficiency than the Al tube. The crashworthiness performance of the GFRP tube increased when the crush length was increased. Babbage et al. [38] investigated the empty and epoxy foam filled hybrid tubes with circle and square sections experimentally. The effect of [±45] or [±75] stacking sequence, composite thickness, and filler on the energy absorption ability were investigated. The circle hybrid tubes having [±45] stacking sequence with the thickest composite wrap and foam-filler absorbed the highest energy. Guden et al. [39] investigated the foam filling effects on the GFRP composite and aluminum/composite hybrid tubes under axial loading. Although the foam filling caused axial splitting of the composite wrap, it did not affect the crash force and energy absorption values. Crash force values of empty hybrid sections was higher than the total of the crush force values of empty metal and composite tubes.

Numerical studies were also conducted to model the crash performance of GFRP tubes. Subbaramaiah et al. [40] examined the crash behavior of top-hat structures via LS-DYNA using material model MAT_54, exhibiting similar results with experiments. El-Hage and Mallick [41] modeled hybrid square tubes made of aluminum and GFRP under axial loading, where material model MAT_54 was used for GFRP in LS-DYNA. They investigated the tubes having fiber orientations of [30], [45], [60], [75], and [90]. The highest absorbed energy values were observed in the hybrid tube with a [±90] stacking sequence. The thinner aluminum tubes showed higher crashworthiness behavior than the thicker tubes in terms of crush resistance. Although the hybrid tubes performed better energy absorption (EA) performance than the aluminum tubes, their SEA values were less than or equal to that of the aluminum tubes. Han et al. [42] evaluated the EA behavior of hybrid tubes with material model MAT_54 in LS-DYNA. They investigated how hybrid tubes deformed when subjected to quasi-static and axial dynamic impact loads. The hybrid tube with the $[0]_4$ orientation absorbed the highest energy among all the tubes. Energy absorption was affected by length, composite thickness, and loading condition. The effects of tube filler, tube geometry, and thickness on the SEA of GFRP, metal, and hybrid tubes were investigated by Zhang et al. [43]. PU foam filling in GFRP tubes performed better than Al foam filling. Nejad et al. [44] employed unidirectional glass-carbon fiber-reinforced epoxy resin to create the hybrid composite tube using the pultrusion process. The results of their finite element analysis (FEA) model in ABAQUS showed good agreement with experimental results. According to their findings, choosing the best trigger mechanism leads to progressive collapse and a more than 35% increase in SEA. Mansor et al. [45] investigated the crashworthiness of hybrid Al-GFRP tubes with different fiber orientations under dynamic loading conditions. According to their FEA model, SEA increased as the thickness of the GFRP and Al walls increased. When the hybrid tube was progressively crushed, the internal energy of the aluminum tube was greater than that of the GFRP tube.

Various analytical and theoretical methods, in addition to experimental and numerical approaches, were also found to be successful in estimating the energy absorption capacity of composite tubes. Generally, researchers focused on the analytical investigation of the mean crush force of tubular sections by employing different geometries such as square [46, 47], circular [48–50], and conical cross sections [50–52]. Mamalis et al. [46, 48] developed analytical models for GFRP tubes. Their results demonstrated that square tubes had a similar deformation mechanism as compared to circular tubes, with the exception of a minor variation in crush zone dimension. In order to forecast the mean crush forces for cylindrical composite tubes with stable progressive failure mode, Solaimurugan and Velmurugan [49] and Boria et al. [50] compiled and validated the earlier analytical models. They discovered that the difference between the analytical mean force predictions and test values was less than 20%. For the circular metal tubes that were externally reinforced with FRP layers, Hanefi and Wierzbicki [53] developed a simplified analytical model. The membrane energy in the metal tube, the energy in the FRP layers, and the bending energy between the walls of the hybrid tube affected the main crushing/failure mechanisms in hybrid tubes. The mean force and the wave length of local folding were estimated in terms of geometric and material characteristics, such as tube thickness, tube diameter, and yield strengths. An empirical Cowper-Symonds constitutive law was developed by Song et al. [35] to take into account the strain rate effect of metallic tubes under dynamic crushing. Wang and Lu [54] developed mathematical formulas for simulating the impact of the layup angle of fiber-reinforced plastic (FRP) layers by taking into account the crushing mechanisms, and the relative errors of the projected mean force were less than 22% compared to the experimental results. By taking into account the impact of arbitrary ply patterns, Mirzaei et al. [34] developed an analytical model with a maximum error of 26.08% between predicted and experimental results. They discovered that the orientation of FRP layers, FRP layer thickness, and the mechanical characteristics of metal components all significantly influence the collapse modes of hybrid tubes, which are dominated by metallic components.

Researchers aimed to investigate the relationship between the geometric parameters of the hybrid crash tubes. Studies showed that tubes with circular geometry lead to progressive deformation, which results in a better energy absorption performance when compared to other tubes with the same length. Also, the effect of foam filling was investigated to improve the energy absorption ability. It was found that the foam-filled composite tubes performed better crash performance than the empty composite tubes. The foam filling material used in the earlier studies was usually either Al foam or PU foam. In this study, the effect of honeycomb filling in hybrid crash tubes is investigated for the first time in the literature through the use of both experimental and numerical methods.

The paper is organized as follows: Sect. 2 describes the energy absorption parameters applied in the study. Experimental studies on composite and hybrid structures are described in Sect. 3, and the details of the Finite Element Analysis (FEA) model is given in Sect. 4. The crashworthiness results obtained from the experiments and their comparison with the FEA are presented in Sect. 5. Moreover, the effect of honeycomb filling of hybrid tubes is discussed in Sect. 5. The conclusions drawn from this study are listed in Sect. 6.

2 Crashworthiness metrics used in energy absorber design

Extensive effort has been performed to understand the impacts of cross section and material types on the crashworthiness of the energy absorbers. The effects of cross section and type of materials were examined using the crashworthiness parameters such as total absorbed energy (EA), specific energy absorption (SEA), initial peak crush force (IPCF), mean crush force (MCF), and crush force efficiency (CFE).

2.1 Total energy absorption (EA)

The area under the load–displacement curve is used to calculate EA. Therefore, EA can be obtained using the following formula as

$$\mathrm{EA} = \int_0^{x_c} F \, \mathrm{d}x \tag{1}$$

where F is the crushing force and x_c is the cutoff displacement.

2.2 Specific energy absorption (SEA)

For energy absorbers, absorbed energy per unit mass is a significant parameter. It is named the SEA and can be expressed as:

$$\mathrm{SEA} = \frac{\text{Total Energy Absorbed}}{\text{Total Mass}} = \frac{EA}{m} \tag{2}$$

where m is the mass of the structure.

2.3 Initial peak crush force (IPCF)

The highest force at which the initial fold starts is known as the initial peak crush force. From the load–displacement graph, the first peak is used to define the initial peak crush force.

2.4 Mean crush force (MCF)

The ratio of the EA to the cutoff deformation, x_c, determines the mean crush force, MCF, which can be expressed by the following equation:

$$\mathrm{MCF} = \frac{EA}{x_c} \tag{3}$$

2.5 Crush force efficiency (CFE)

The ratio of MCF to IPCF is known as the CFE which can be expressed as:

$$\mathrm{CFE} = \frac{\mathrm{MCF}}{\mathrm{IPCF}} \tag{4}$$

The ultimate goal of an energy absorber design is to obtain large SEA, MCF, and CFE but small IPCF values.

3 Experimental study

3.1 Material characterization tests

Composites could be manufactured by various techniques in order to satisfy design requirements. Hand layup is a typical fabrication technique to manufacture GFRP and hybrid tubes. In order to determine the mechanical properties of composites to be used in the FEA model, tensile, compression, and shear tests were conducted. These mechanical properties (given in Table 1) are needed in order to define the material card in LS-DYNA. ASTM standards were followed for the tensile, compression, and shear tests. These tests were conducted at Izmir Institute of Technology utilizing a Shimadzu™AG-IC Series universal test machine with a maximum capacity of 100 kN. The geometries of the test specimens are shown in Fig. 1. Material density and fiber volume fraction values were obtained from the composite manufacturer (ACME Kompozit Company) as 1.5 g/cm^3 and 33%, respectively.

Test specimens used in the tensile, compressive, and shear tests are shown in Fig. 2. The values of the length and the width of test specimens are given in the test standards for the specimens with 0° and 90° orientations. ASTM-D3039 tensile tests were conducted using specimens with 0° and 90° fiber orientation at a speed of 2 mm/min. Test specimen dimensions in ASTM-D3039 are 250 mm × 15 mm × 2 mm, for 0° fiber orientation and 175 mm × 25 mm × 2 mm for 90° fiber orientation. Test specimens consist of two regions: gauge length, in which failure is expected to occur, and the two end regions with tabs that are clamped to the test machine. For the tensile test, test specimens were prepared according to the ASTM-D3039 standard. Samples were marked with special markers (using special labels or pens that distinguish the marking from the sample color and texture in recorded images) before the mechanical tests were conducted. Each specimen, which was properly centered between the jaws of the tensile testing machine, was pulled with an increasing load until it breaks. The pixel distance (70 mm for 0° specimens and 50 mm for 45° and 90° specimens) between these marks on the tensile test specimens was recorded while the specimens were under tension. Therefore, an accurate strain measurement value can be obtained by measuring the pixel distances. For the test results to be reliable, the fracture zone must remain within the gauge length. Views of the test specimens before the mechanical tests were given on the left side of Fig. 2. Also, the images of the test specimens after the mechanical tests were circled to show the fracture zones on the right side of Fig. 2.

Average tensile strength values were found to be 469.1 MPa and 45.8 MPa for the specimens with 0° and 90° fibre orientation, respectively.

ASTM-D6641 compressive tests were conducted using specimens with 0° and 90° fibre orientation at a speed of 2 mm/min. Test specimen geometry was 140 mm × 12 mm × 2 mm for the specimens. Test results are shown in Fig. 3. Average compression strength values were found to be 542.51 MPa and 82.70 MPa for the specimens with 0° and 90° fibre orientation, respectively.

Shear tests were conducted according to ASTM-D3518 standard using specimens with [±45] fibre orientation at a speed of 2 mm/min. Test specimen geometry was 175 mm × 25 mm × 2 mm. The average tensile strength was found to be 101.9 MPa.

3.2 Quasi-static crushing test of the tubes

INSTRON 600 LX with a load capacity of 600 kN was used for the quasi-static crash tests of aluminum, composite, and hybrid tubes at TOBB University of Economics and Technology. The tubes were attached to the mandrel using the

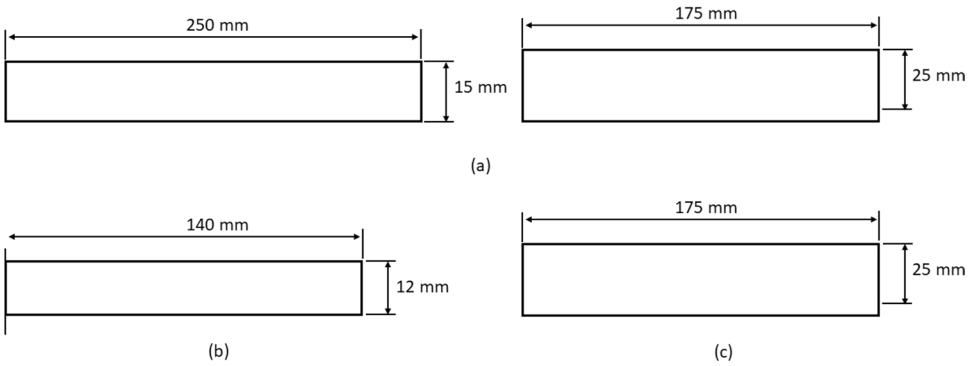

Fig. 1 Specimen geometries for **a** ASTM-D3039 tensile test **b** ASTM-D6641 compressive test **c** ASTM-D3518 shear test

Table 1 Material properties and tests required for determining the parameters used in MAT_54

Property	Description	Test	Standard
EA	Modulus in longitudinal (fiber) direction	0° tensile test	ASTM D3039
EB	Modulus in transverse direction	90° tensile test	ASTM D3039
PRCA	Major Poission's ratio	0° tensile test	ASTM D3039
PRBA	Minor Poission's ratio	90° tensile test	ASTM D3039
XT	Longitudinal tensile strength	0° tensile test	ASTM D3039
YT	Transverse tensile strength	90° tensile test	ASTM D3039
XC	Longitudinal compressive strength	0° compression test	ASTM 6641
YC	Transverse compressive strength	90° compression test	ASTM 6641
SC	Shear strength	Shear test	ASTM D3518
GAB	Shear modulus	Shear test	ASTM D3518

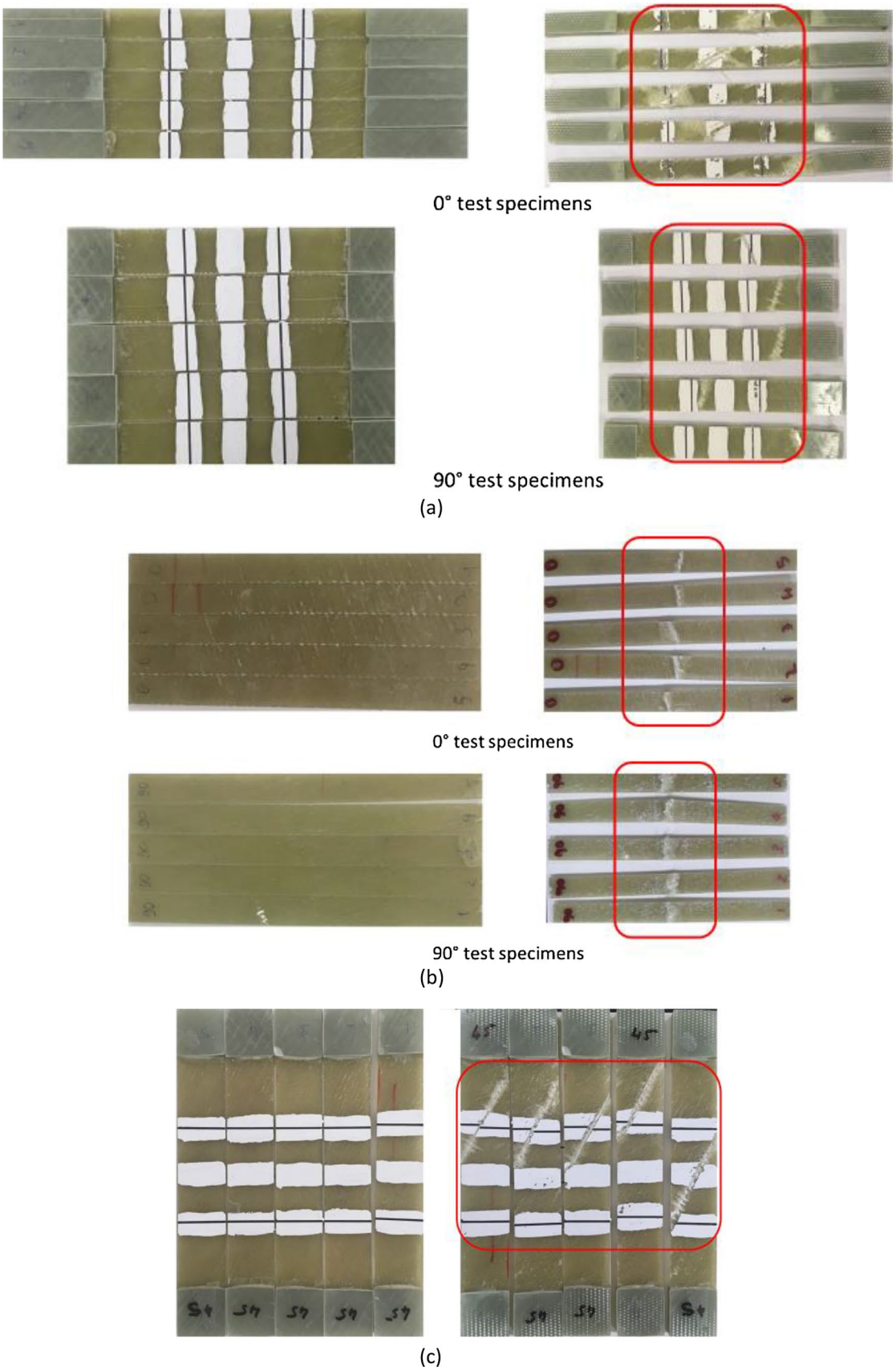

Fig. 2 Test specimens before and after mechanical tests **a** ASTM-D3039 tensile test **b** ASTM-D6641 compressive test **c** ASTM-D3518 shear test

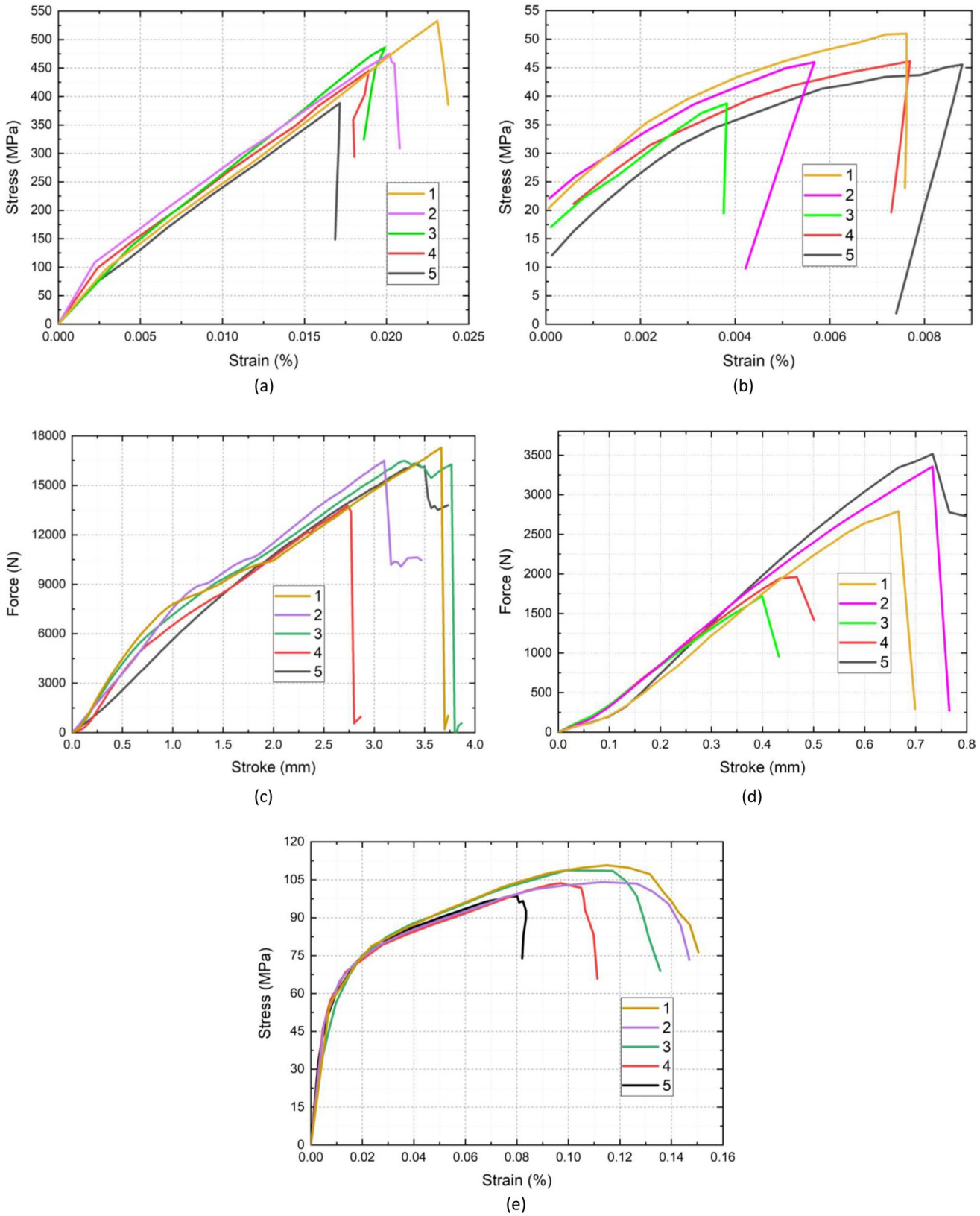

Fig. 3 Test results of **a** ASTM-D3039 tensile test for 0° specimens **b** ASTM-D3039 tensile test for 90° specimens **c** ASTM-D6641 compressive test for 0° specimens **d** ASTM-D6641 compressive test for 90° specimens **e** D3518 shear results of 45° specimens

bottom plate, which prevents the tubes from shifting during axial loading, as shown in Fig. 4.

The circular tubes with a length of 100 mm were used in the experimental studies. For the aluminum tube, Al 6082-T86 alloy with a wall thickness of 2 mm and a diameter of 80 mm was used. GFRP tubes were manufactured with 2.76 mm wall thickness and 85.5 mm diameter. Composite tubes were composed of 6 GFRP fabric layers with $[\pm 75]_3$ orientation and manufactured by using 6 plies of 330 UD by hand layup method. GFRP/hybrid and Al 6082-T6 tubes were supplied from Acme Kompozit and Ozdemirler Metal, respectively.

In hybrid tubes, aluminum tubes with 2 mm wall thickness and 80 mm diameter were used. Aluminum tubes were wrapped with GFRP to produce hybrid tubes with an 85.5 mm diameter. Honeycombs were made of aluminum 3005/H19 with a cell size of 10.39 mm and foil thickness of 50 microns. All the specimens used in the experimental study are shown in Fig. 5. GFRP and hybrid tubes were filed to have a chamfer before the crush tests. Experimental and computational studies related to the effect of trigger mechanisms on the energy absorption capacity of composite tubes under axial compression can be found in the literature [55, 56]. Applying a 45° chamfer to one end of the tube is a traditional method for introducing a trigger mechanism, which could result in a progressive failure. Therefore, we applied a chamfer to one end of the tube to observe the progressive failure of GFRP tubes in this study. Details of the chamfering process can be seen in Fig. 6.

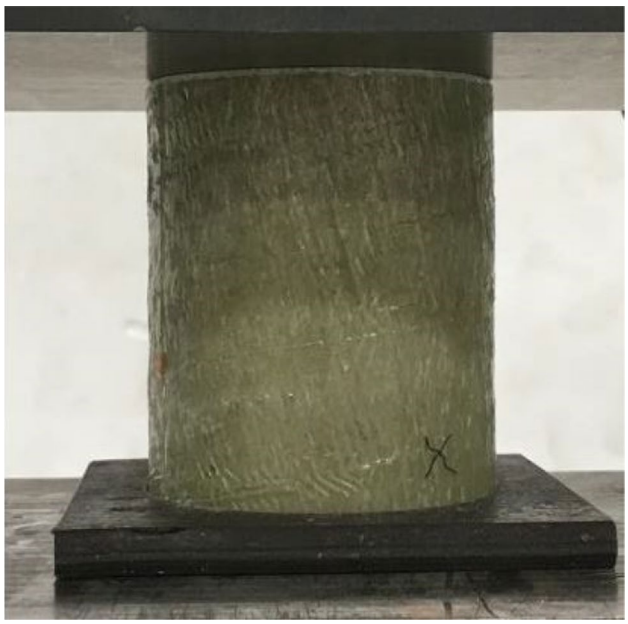

Fig. 4 Hybrid tube with bottom plate

3.3 Experimental results

In the experiments, the tubes were compressed by the upper plate with a velocity of 2 mm/min. Tubes were compressed up to 60 mm of deformation, which corresponds to 3/5 of their original length. Deformed views of the specimens are shown in Fig. 7. Aluminum tubes showed progressive folding. Failure began from the upper part of the tube, and cracks were observed in GFRP and hybrid tubes. The force-displacement graphs of the tubes obtained from the experiments are displayed in Fig. 8. When Fig. 8a is compared with Fig. 8b–d along with the results provided in Table 2, it is observed that the crashworthiness metrics of GFRP and hybrid tubes are better than those of aluminum tubes. Table 2 shows that CFE value of GFRP is significantly larger (almost twofold) than those of Al tubes as well as hybrid tubes. When the SEA values of the tubes are compared, the GFRP tubes displayed the best performance followed by hybrid and Al tubes.

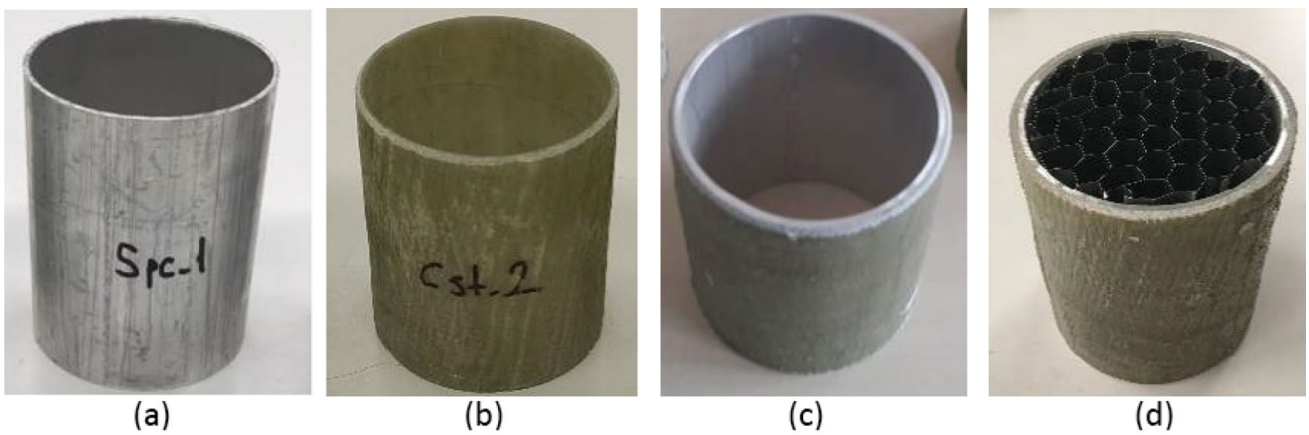

Fig. 5 Test specimens **a** aluminum 6082-T6 tubes **b** GFRP tubes **c** hybrid tubes **d** honeycomb filled hybrid tubes

Fig. 6 Chamfering process of the hybrid tube

4 Finite element modeling

4.1 Construction of the FEA model

Finite element analysis (FEA) models are generated using LS-DYNA software which is commonly used for investigating the crushing response of fiber-reinforced plastic tubes. Figure 9 shows the FEA model of the honeycomb filled hybrid tubes used in this study. The composite tube is modeled using 3-layers in LS-DYNA. Four-node quadrilateral Belytschko-Tsay shell elements are used in the model. Hourglass control is applied to the fully-integrated elements. Each layer is modeled with 2 through-thickness integration points defining 2 different stacking sequences. During the deformation, the upper and lower platens were represented as two rigid surfaces. The lower plate is fixed to the ground and the upper one is subjected to compression with a speed of 0.2 mm/ms. To reduce the computational run time, mass scaling is applied ensuring that the model demonstrates quasi-static compression (i.e., kinetic energy is less than 10% of internal energy). The LAMSHT variable on the CONTROL_SHELL card is activated to use of laminated shell theory in the calculations of laminate stiffness through the thickness.

4.2 Trigger mechanism

In order to have a similar deformation behavior with the experiments, usually chamfer and trigger mechanisms is employed in the FEA models to enhance progressive crushing [55, 57–60]. The trigger mechanism used in this study is similar to the one used in the works of Huang and Wang [57] as well as Rabie and Ghasemnejad [58]. The trigger mechanisms are generally implemented in the form of a chamfer on the upper part of the tube to decrease the initial peak force and obtain a progressive failure. In order to converge to experimental results, one row of elements is defined as a trigger (a length of 1.25 mm, red color in Fig. 10), and three rows of elements are defined as neighboring the trigger (a length of 3.75 mm, green color in Fig. 10). Trigger elements have a thickness of 0.8 mm and neighboring elements have a thickness of 0.92 mm. Although 5°, 10° and 15° inward-chamfering mechanisms are applied in the study of Rabie and Ghasemnejad [58], FEA results converged to experimental results when 0° trigger chamfering mechanism is utilized in this study.

4.3 Contact definitions

Tiebreak contact algorithms are applied to model the contact between the layers that interact with each other

Table 2 Experimental results of aluminum, GFRP, empty hybrid and honeycomb filled hybrid tubes

	Peak force (kN)	Mean force (kN)	CFE	EA (kJ)	Mass (kg)	SEA (kJ/kg)	Cost ($)
Al1	83.28	39.38	0.46	2.363	0.123	19.21	0.6
Al2	82.45	36.67	0.46	2.200	0.127	17.32	0.6
Al3	80.88	39.35	0.48	2.361	0.125	18.89	0.6
GFRP1	74.96	66.07	0.88	3.964	0.116	34.172	71
GFRP2	61.96	50.68	0.82	3.041	0.104	29.240	71
GFRP3	56.81	51.08	0.91	3.108	0.106	29.320	71
Hybrid1	187.76	85.95	0.46	5.157	0.218	23.655	71.6
Hybrid2	211.38	82.45	0.39	4.947	0.218	22.693	71.6
Hybrid3	157.45	76.32	0.48	4.579	0.211	21.702	71.6
Honey1	161.01	72.58	0.45	4.355	0.238	18.298	72
Honey2	161.76	77.91	0.48	4.675	0.238	19.642	72
Honey3	190.64	83.18	0.44	4.991	0.239	20.882	72

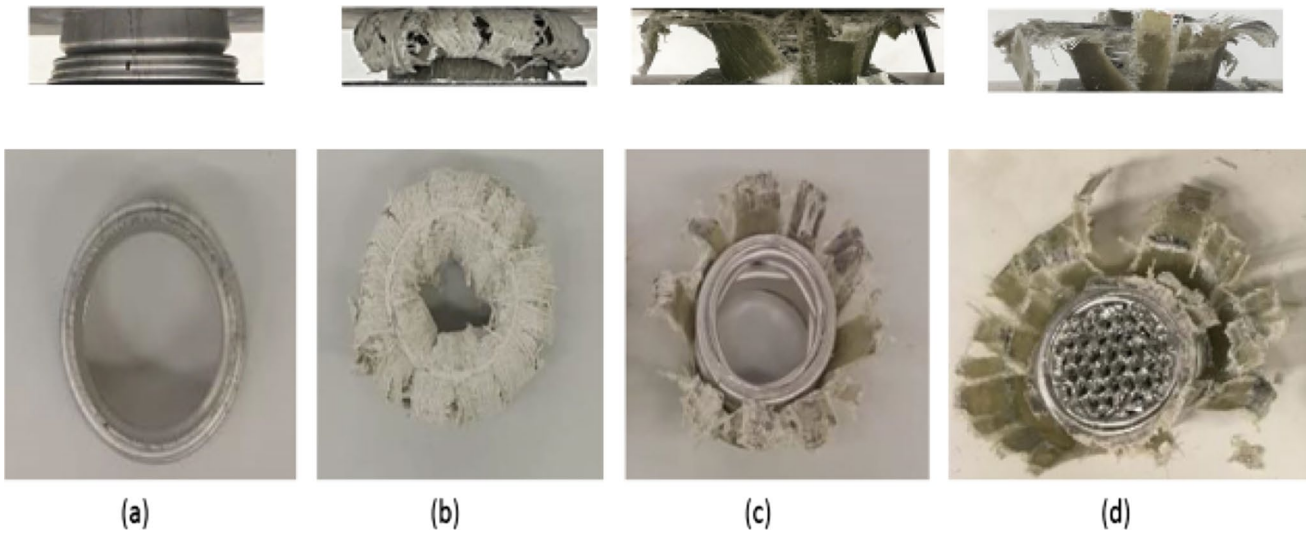

Fig. 7 Deformed shape of the specimens corresponding to 60 mm deformation **a** Aluminum 6082 T6 tube **b** GFRP tube **c** hybrid tube **d** honeycomb filled hybrid tube

while preventing interpenetration. The contact between the upper plate and the tube, as well as the contact between the honeycomb and the aluminum tube, is defined using the CONTACT_AUTOMATIC_ SURFACE_TO_SURFACE card, whereas the contact of the tube within itself is defined using CONTACT _AUTOMATIC_SINGLE_SURFACE card. Both static and dynamic friction coefficients are specified as 0.25 for the CONTACT_AUTOMATIC_SURFACE_TO_SURFACE card. Both static and dynamic friction coefficients for contact algorithms are specified as 0.4 for the CONTACT_AUTOMATIC_SURFACE_TO_SURFACE_ TIEBREAK card.

The CONTACT_AUTOMATIC_SURFACE_TO_SURFACE_TIEBREAK card is used with option 8 to model delamination between the layers of the composite tube, between the composite tube and the aluminum tube, and between the composite tube and the honeycomb. According to this contact method, the failure initiates when the distance between the two elements in contact (PARAM), the normal stress (NFLS), and the shear stress (SFLS) values reach their specified values. After a parametric analysis for the 3-layer model, the maximum normal stress for the tiebreak contact is set to NFLS=65 MPa, and shear contact stress for the tiebreak contact is set to SFLS=90 MPa. The critical value of the contact distance is set to PARAM=0.11 mm. NFLS is set to 27 MPa, and SFLS is set to 50 MPa for the tiebreak contact between the aluminum and GFRP tube in the hybrid tube analysis.

4.4 Material models

Material models MAT_54 and MAT_55 were used to model the composite structures. The failure model used in MAT_54 is the Chang-Chang matrix failure criterion, while the Tsay-Wu criterion is used in MAT_55. In this study MAT_ENHANCED_ COMPOSITE_DAMAGE material model with Chang-Chang criteria (MAT_54 model) is used to simulate the deformation pattern of GFRP tubes. Zhang et al. [43], Huang and Wang [57], Boria et al. [61], Boria et al. [62], Reuter et al. [63], and Meric and Gedikli [64] used the orthotropic material model with MAT_54 "MAT_ENHANCED_COMPOSITE_DAMAGE" card with the failure criteria of Chang-Chang. According to Chang- Chang criteria, failure begins when the conditions given below are met [65]:

For the tensile fiber mode,

$$\left(\frac{\sigma_1}{XT}\right)^2+\beta\left(\frac{\tau_{12}}{SC}\right)^2-1 \tag{5}$$

$$\left(\frac{\sigma_1}{XC}\right)^2-1 \tag{6}$$

$$\left(\frac{\sigma_2}{YT}\right)^2+\left(\frac{\tau_{12}}{SC}\right)^2-1 \tag{7}$$

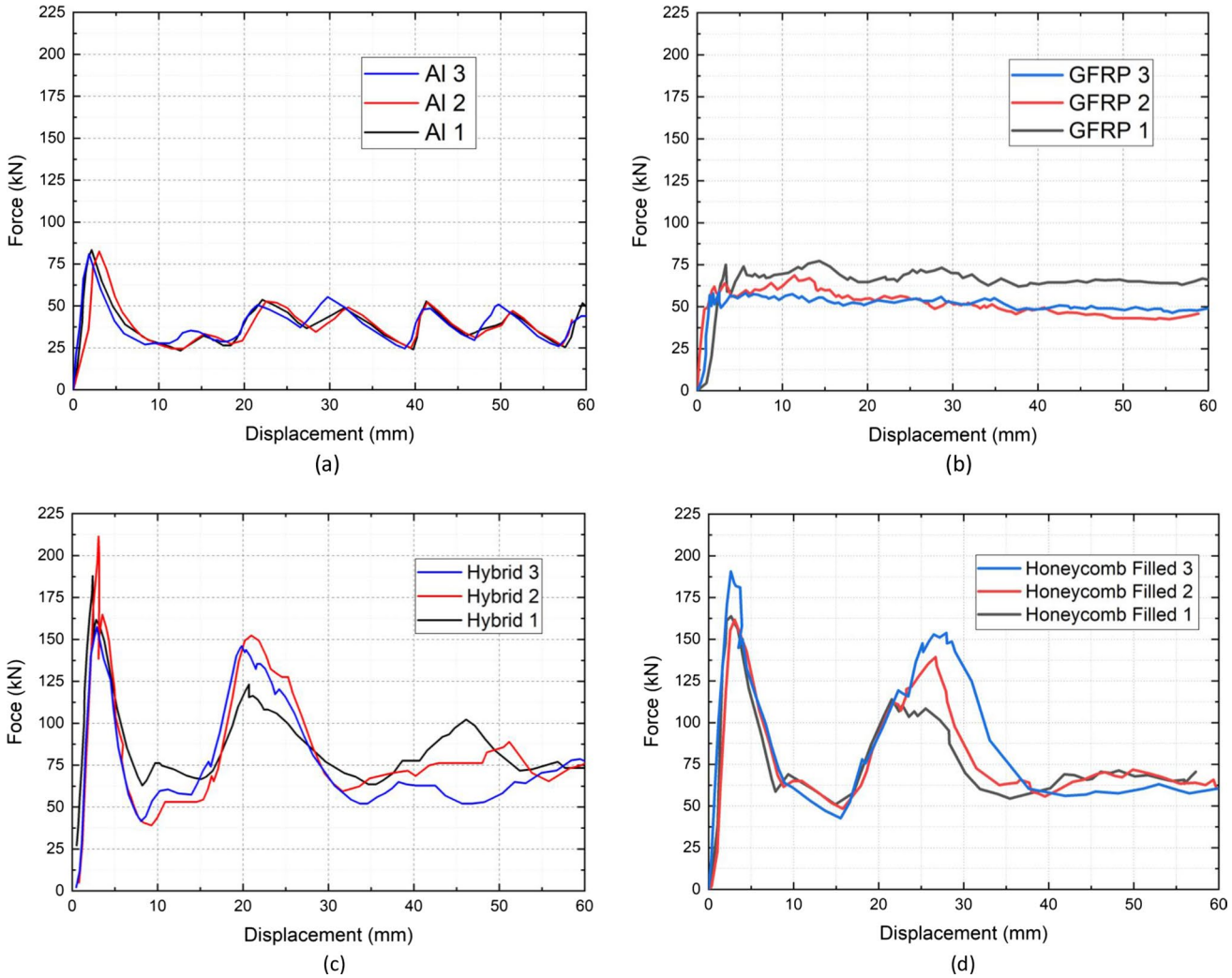

Fig. 8 Force-displacement behavior of the tested specimens **a** Aluminum 6082 T6 tube **b** GFRP tube **c** hybrid tube **d** honeycomb filled hybrid tube

$$\left(\frac{\sigma_2}{2SC}\right)^2 + \left[\left(\frac{YC}{2SC}\right)^2 - 1\right] + \frac{\sigma_2}{YC} + \left(\frac{\tau_{12}}{SC}\right)^2 - 1 \tag{8}$$

where XT is longitudinal tensile strength, XC is longitudinal compressive strength, SC is shear strength, and YT is transverse tensile strength.

In the MAT_54 material model, 10 parameters are determined according to material characterization tests and 7 numerical parameters could be tuned according to the literature or conducting a calibration study to resemble the deformation behavior of experimental results. The material parameters obtained with mechanical tests and numerical parameters are given in Tables 3 and 4, respectively.

In the calibration procedure, the four material model parameters, maximum strain for fiber compression DFAILC, maximum strain for fiber tension DFAILT, maximum strain for matrix straining DFAILM, and maximum tensorial shear strain DFAILS are investigated. These parameters are varied until the consistency is observed in the force-displacement curve and the deformation views. The calibrated values for DFAIL parameters are as follows: DFAILC = −0.7, DFAILM = 0.85, DFAILT = 0.05, and DFAILS = 0.3.

Al 6082-T6 alloy is modeled with MAT_24_PIECEWISE_LINEAR_PLASTICITY card in LS-DYNA [65]. The density of the material is $\rho = 2.6$ g/cm^3; the Poisson's ratio is $\nu = 0.3$; the Youngs modulus is $E = 69$ GPa [66]. Also, an effective true stress- effective true plastic strain curve is defined in MAT_24 utilizing the values given in Table 5 for aluminum 6082 [66].

Similarly, MAT_24 is used to model aluminum honeycomb filler which has a cell size of 10.39 mm. The Young's modulus is E=298 MPa, the Poisson's ratio is $\nu = 0.3$, and the yield strength was $\sigma_y = 250$ MPa.

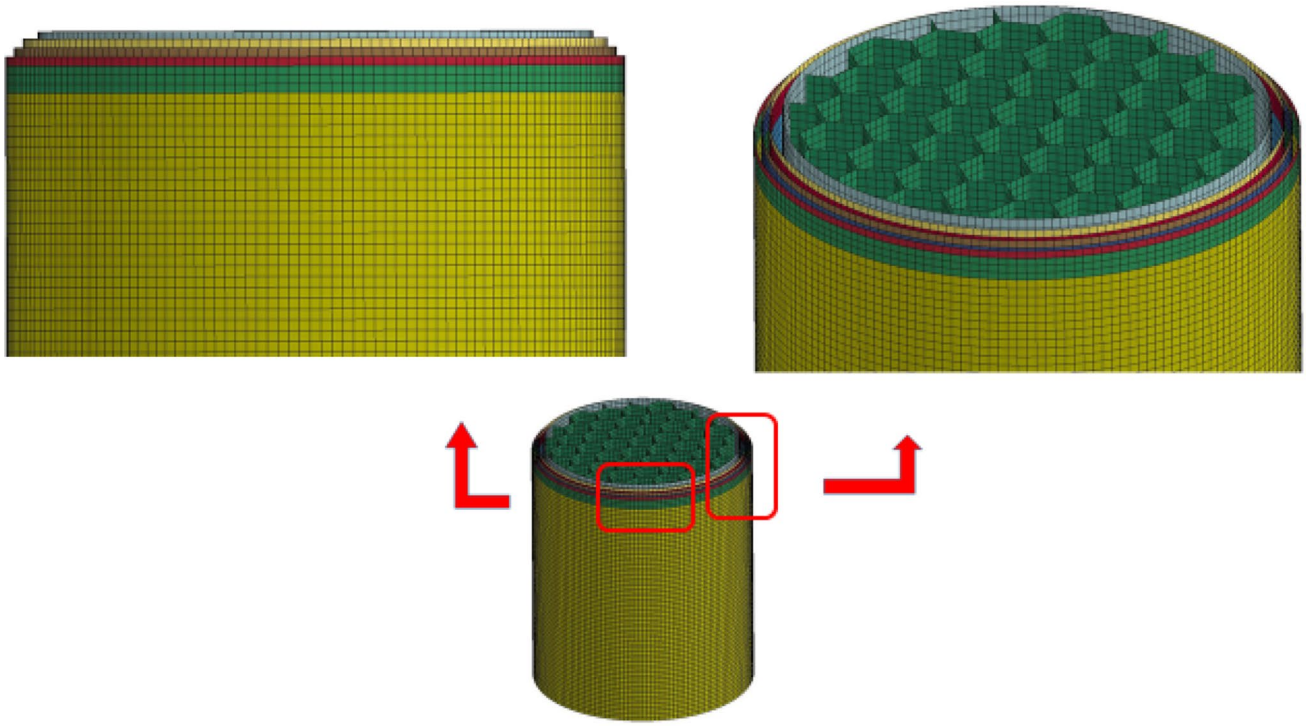

Fig. 9 FE model of honeycomb filled hybrid tube

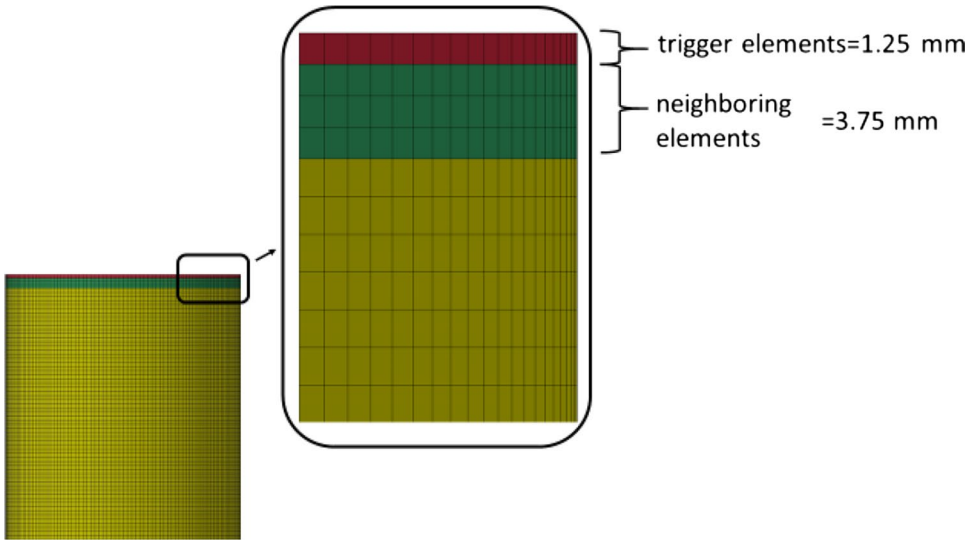

Fig. 10 Trigger mechanism applied to the FE model

4.5 Mesh convergence study

Mesh size sensitivity analysis is performed to find the acceptable mesh size for the computationally efficient and accurate model. The feasible result was obtained at the element size of 1.5 mm, as shown in Fig. 11.

5 Results and discussion

5.1 Aluminum tubes

Energy absorption results and the force-displacement graphs are given to compare the results of FEA and experiments.

Table 3 Material parameters used in the MAT_54 card in LS-DYNA

Property	Description	Test
ρ	Density	1.5 g/cm^3
EA	Modulus in longitudinal (fiber) direction	21.55 GPa
EB	Modulus in transverse direction	6.92 GPa
GAB	Shear modulus	5.48 GPa
PRCA	Major Poission's ratio	0.24
PRBA	Minor Poission's ratio	0.13
XT	Longitudinal tensile strength	469.1 MPa
XC	Longitudinal compressive strength	542 MPa
YT	Transverse tensile strength	45.8 MPa
YC	Transverse compressive strength	82.7 MPa
SC	Shear strength	50.95 MPa

Table 4 Numerical parameters used in the MAT_54 card in LS-DYNA

Property	Description	Values
ALPH	Shear stress parameter for the nonlinear term	0.0
YCFAC	Reduction factor for compressive fiber strength after matrix compressive failure	2.0
FBRT	Softening for fiber tensile strength	1.0
BETA	Weighting factor for shear term in tensile fiber mode	0.0
TFAIL	Time step size criteria for element deletion	0.0
SOFT	Softening reduction factor for material strength in crashfront elements	0.825
EFS	Effective failure strain	0.0

Table 5 Effective true stress-effective true plastic strain values defined in the MAT_24 card in LS-DYNA [66]

σ_t (MPa)	145	149	157	168	171
ε_p	0.0	0.0158	0.0331	0.0586	0.0664

Figure 12 depicts the deformed views of aluminum specimens at displacements of 20, 40, and 60 mm. Figure 13 explores the load–displacement graphs for aluminum tubes used to compute the energy absorption values given in Table 6, which compares the crashworthiness metrics between the results of FEA with the experiments. It is seen that the errors observed for CFE and SEA are − 8.5% and 11.1%, respectively, which are found to be acceptable for a nonlinear phenomenon like a crush.

5.2 GFRP tubes

Three circular tubes made of GFRP with 2.75 mm wall thickness were tested under axial loading. During experiments, laminate bundles curved in and out along the mid-plane of the wall thickness. Bundle fractures and fronds existed when the GFRP tubes were deformed. Transverse shearing and crack propagation between the bundles and the upper plate dissipated the crushing energy, as observed in the study of Chen et al. [67]. Lamina fronds were observed, including delaminations, fragmentations, and fractures of fiber bundles. Although deformation patterns were similar for all GFRP specimens, the force-displacement behavior of specimen #1 was not compatible with the other two specimens. Therefore it was not included while computing the average values of the crashworthiness metrics. Figure 14 presents a comparison of the deformation views of GFRP tubes obtained through FEA and experiments. It is observed that the deformed views are in close agreement. Moreover, force-displacement characteristics until 60 mm of deformation are depicted in Fig. 15. Specimens exhibit a crushing failure process in terms of bundles and delamination, as observed in both experiments and FEA results, as shown in Fig. 16. Note that lamina fronds and fractures of fiber bundles are observed in both test specimen and finite element model. The lamina bundles deform inward and outward with a stable damage progression.

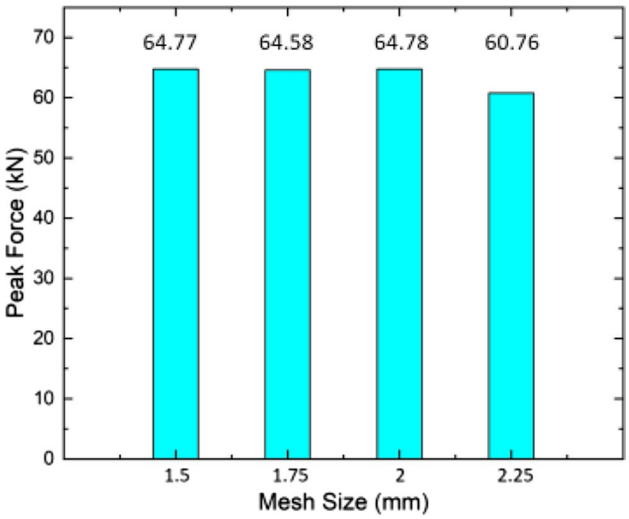

Fig. 11 Mesh size sensitivity analysis

Table 7 displays the comparison of FEA and experimental results. The FEA model shows acceptable accuracy in crashworthiness metrics compared to experimental results. The SEA of the FEA model is 25.24 kJ/kg, while the SEA observed in the tests is 29.28 kJ/kg, and the absolute relative error is 13.8%. The EA of the FEA model is 2.675 kJ, while the EA observed in the tests is 3.074 kJ, and the absolute relative error is 13%. The CFE of the FEA model is 0.69, while the CFE observed in the tests is 0.86, and the absolute relative error is 19.8% which is found to be high compared to the error found in SEA and EA.

Table 6 Comparison of crashworthiness metrics between FEA and experimental results for Al tubes

	Peak force (kN)	Mean force (kN)	CFE	EA (kJ)	Mass (kg)	SEA (kJ/kg)
Test	82.20	38.46	0.47	2.308	0.125	18.47
FEA	83.36	42.75	0.51	2.565	0.125	20.52
Error (%)	− 1.4	11.1	− 8.5	11.1	0	11.1

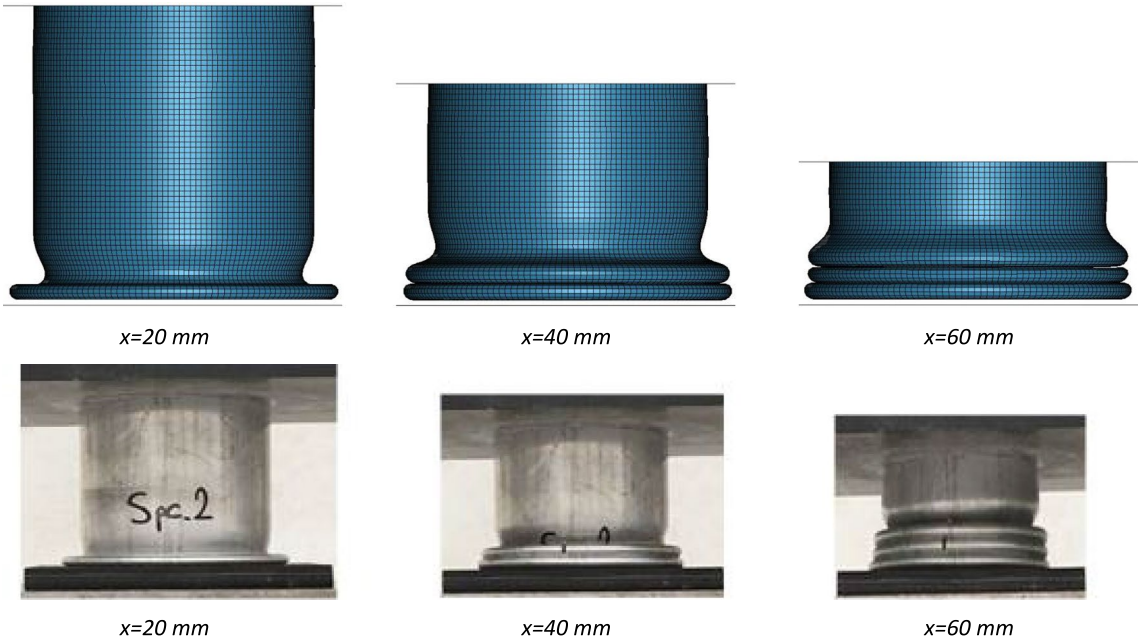

Fig. 12 Comparison of collapse modes of aluminum tubes between experimental and FEA results

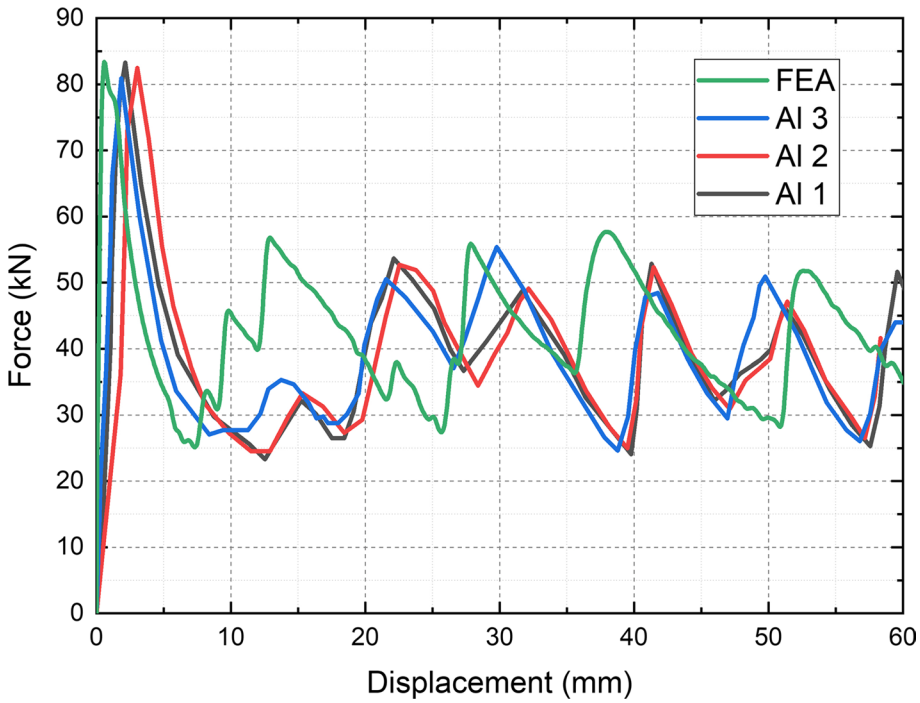

Fig. 13 Crushing load–displacement curves for aluminum tubes

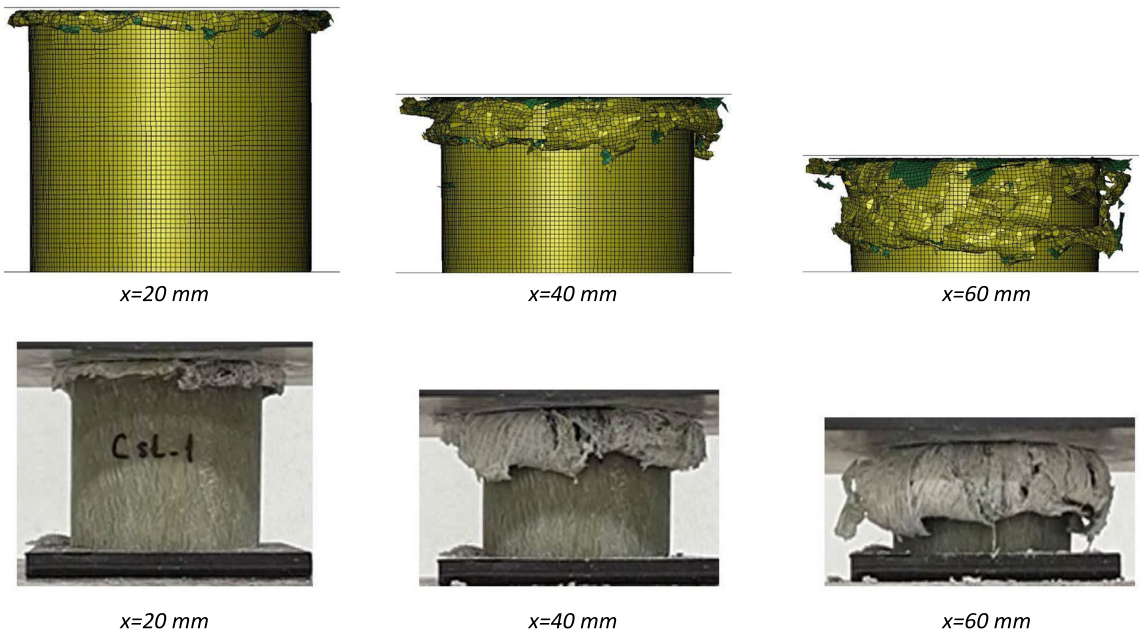

Fig. 14 Comparison of collapse modes of GFRP tubes between experimental and FEA results

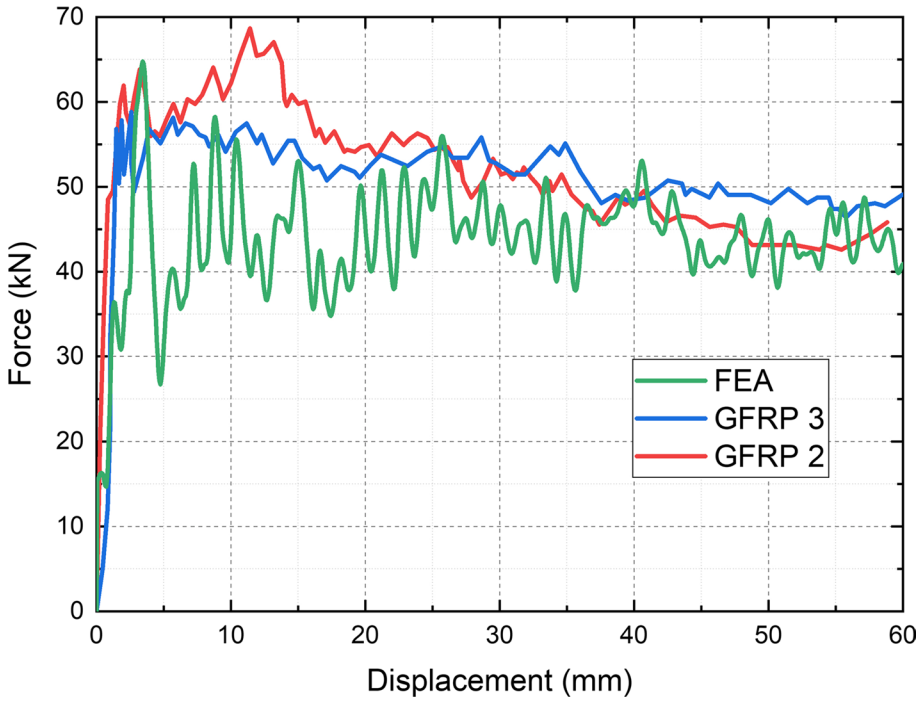

Fig. 15 Crushing load–displacement curves for GFRP tubes

5.3 Hybrid tubes

As shown in Fig. 17, cracks and bundles are initiated at the top of the tube. The crushed lamina bundles deform outward due to the existence of an aluminum tube inside. Furthermore, the FEA model shows delamination and fracture, which propagated along the axial direction similar to the test specimens. The hybrid tube deforms in brittle mode with the propagation of longitudinal inter-laminar cracks. Further observations show that the depth of tears increases when the deformation distance increases. Energy absorption of hybrid tubes is realized through both crack formation and outward delamination in hybrid tubes,

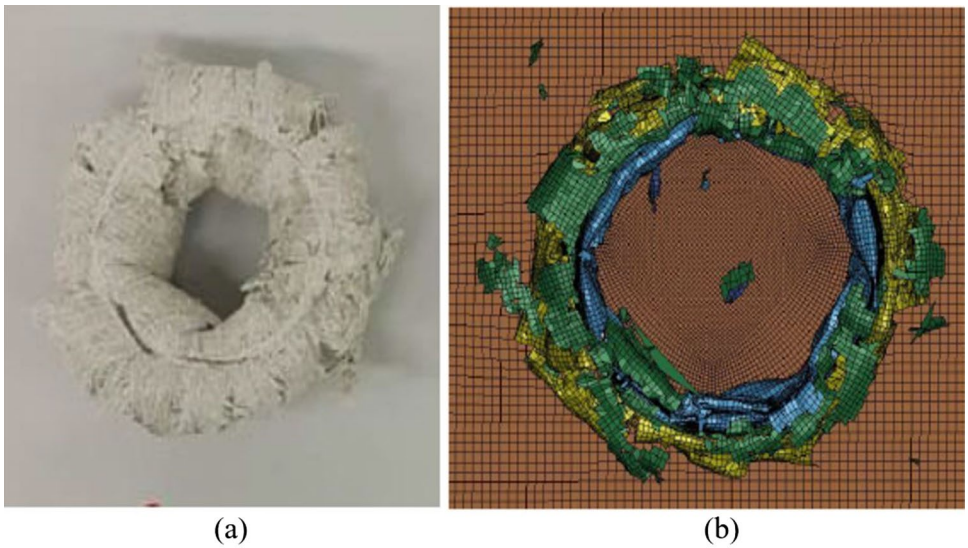

Fig. 16 Deformed view at 60 mm of deformation of GFRP tubes: **a** experiment **b** FEA

Table 7 Comparison of crashworthiness metrics between FEA and experimental results for GFRP tubes

	Peak force (kN)	Mean force (kN)	CFE	EA (kJ)	Mass (kg)	SEA (kJ/kg)
Test	59.39	51.23	0.86	3.074	0.105	29.28
FEA	64.77	44.58	0.69	2.675	0.106	25.24
Error (%)	9.1	− 13.0	− 19.8	− 13	0.95	− 13.8

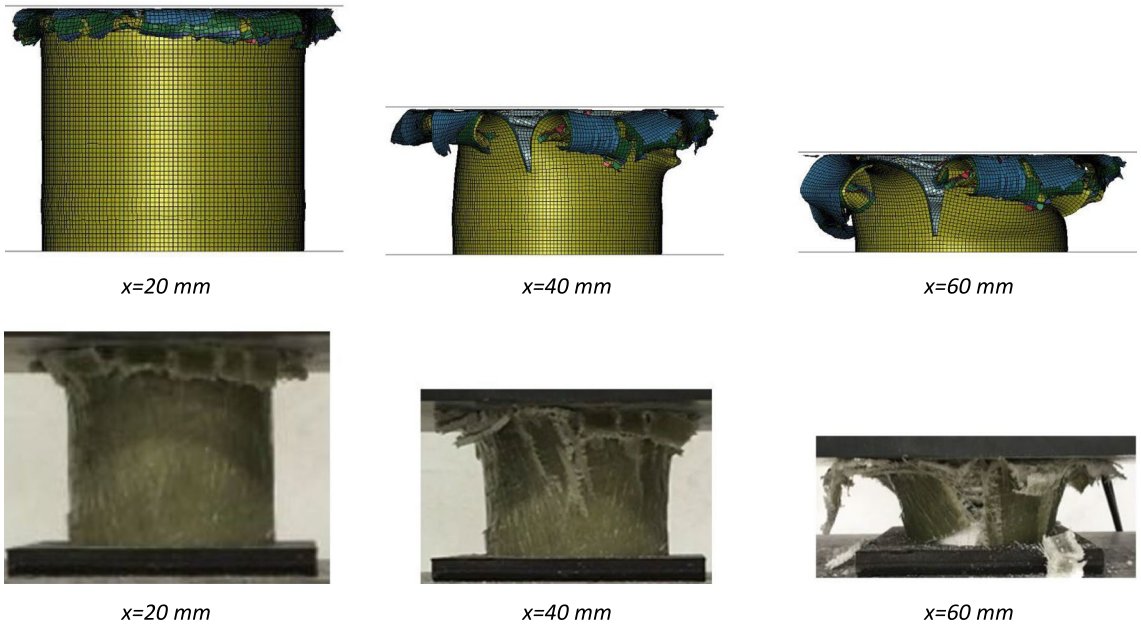

Fig. 17 Comparison of collapse modes of hybrid tubes between experimental and FEA results

unlike the GFRP tubes in which bundles are observed due to a progressive failure mechanism.

All hybrid tube specimens exhibit similar force-displacement behavior, as shown in Fig. 18. As the force increases to its first peak, fibers tend to fail by the formation of cracks since the aluminum tube prevents to form of inward bundles. Also, the primary difference in the force-displacement behavior of the GFRP and the hybrid tubes is the load drop after the peak force is observed. In hybrid tubes, the second peak force occurs when the

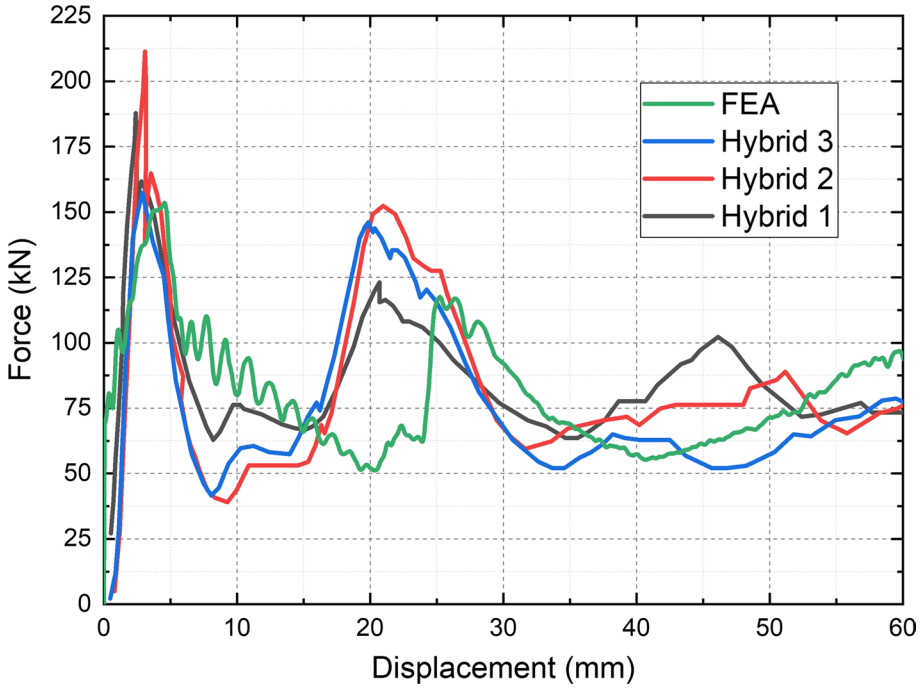

Fig. 18 Crushing load–displacement curves for hybrid tubes

tube deforms 20 mm due to the folding of the aluminum tube inside. The third folding of the aluminum tube causes the third peak force for hybrid tube specimens #1 and #2, although the third peak is not observed clearly for specimen #3.

The force-displacement graph obtained using FEA for the hybrid tube shows a lower initial peak load than the test specimens, as shown in Fig. 18. At the beginning stage of deformation, average experimental results increase up to a peak value near 185 kN, whereas the FEA value of the first peak is 153 kN. After the first peak, the crash force decreases to a minimum value and then increases to form a second peak force of around 140 kN for the average experimental results. The second peak value for the FEA result is 117 kN. Crashworthiness metrics for the FEA and test results are summarized in Table 8. Again, the agreement between the FEA and experimental results is found to be acceptable.

The failure and delamination modes observed in the FEA of hybrid tubes closely resemble the test results. Figure 19 shows the deformed views of hybrid tubes at the crushing displacement of 60 mm. Folding for aluminum tube and crack formations for GFRP composite are observed when the hybrid tube deformed axially.

5.4 Honeycomb filled hybrid tubes

Figure 20 shows the numerical and experimental deformation process of the honeycomb filled tubes at 20 mm, 40 mm, and 60 mm deformation, respectively. All specimens exhibit a failure process, which includes cracks and delamination, as shown in Fig. 20. According to the force-displacement graph in Fig. 21, deformed views of the tubes and collapse modes, it can be concluded that FEA results are in line with the experimental results. It can be observed that force-displacement graphs for the honeycomb filled hybrid tubes showed similar behavior as in the hybrid tubes. Note that the average experimental results increase up to a peak value near 171 kN, whereas the FEA value of the first peak is 155 kN. The second peak force for average experimental results is around 135 kN, whereas the second peak value for the FEA result is 115 kN. Crashworthiness metrics for the FEA and test results are summarized in Table 9, which shows that the EA and SEA of honeycomb filled hybrid tubes are lower than those of non-filled tubes. The IPCF, MCF, and CFE values obtained for honeycomb filled tubes are found to be similar to non-filled tubes. Therefore honeycomb filling is not found to be an effective way to improve the crashworthiness performance of the hybrid tubes. Specimens exhibit a crushing failure process in

Table 8 Comparison of energy absorption values between simulation and experimental results of hybrid tubes

	Peak force (kN)	Mean force (kN)	CFE	EA (kJ)	Mass (kg)	SEA (kJ/kg)
Test	185.53	81.57	0.44	4.894	0.216	22.66
FEA	153.54	82.08	0.53	4.925	0.230	21.41
Error (%)	− 17.2	0.6	20	0.6	6.5	− 5.5

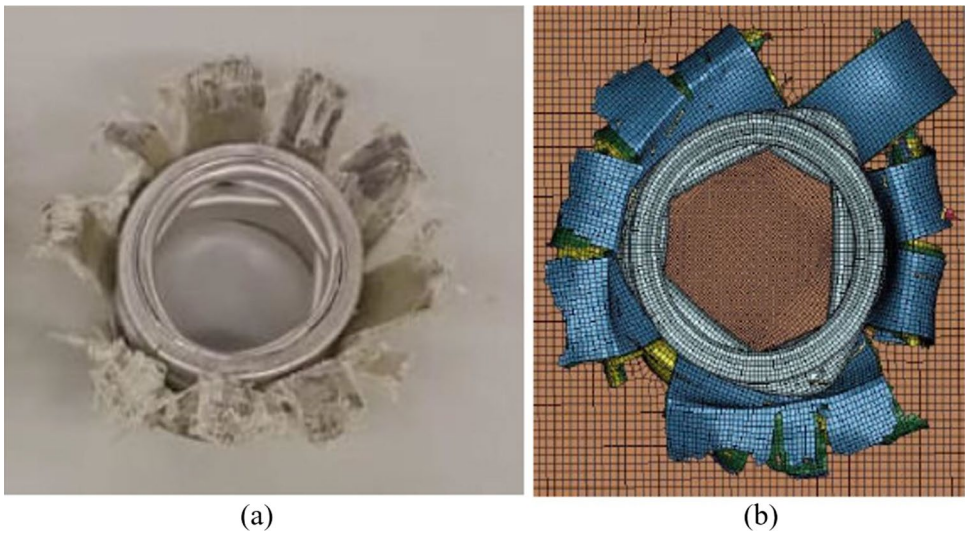

Fig. 19 Deformed view at 60 mm of deformation of empty hybrid tubes: **a** experiment **b** FEA

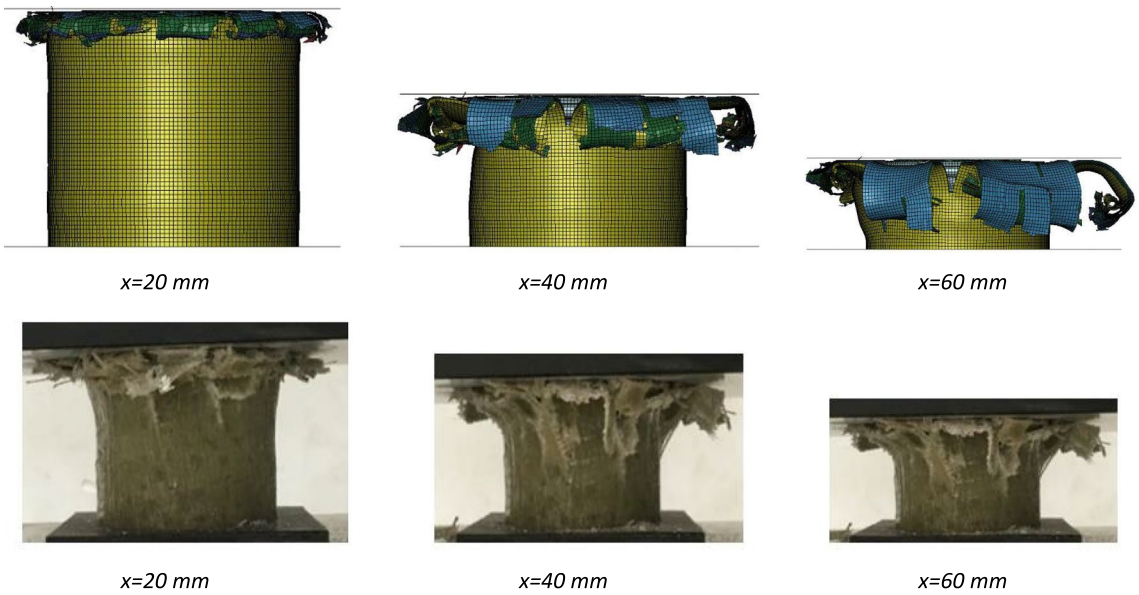

Fig. 20 Comparison of collapse modes of honeycomb filled hybrid tubes between experimental and FEA results

terms of bundles and cracks, as observed in FEA results. Failure mechanisms for honeycomb filled tubes are found to be consistent with the test results at 60 mm deformed views, as shown in Fig. 22.

6 Conclusions

In this paper, the quasi-static crushing response of empty Al, empty GFRP, empty hybrid tubes, and honeycomb filled hybrid tubes were investigated experimentally and numerically. A validated finite element model provides valuable information, such as the deformation patterns and failure mechanisms in every step of the crushing process. For example, a deformation pattern comparison related to four different configurations can be seen in Fig. 23. The main focus of this study was on the effect of honeycomb filling on the crashworthiness behavior of hybrid tubes. The significant findings of this study can be summarized as:

- when the crashworthiness performances of empty Al and empty GFRP tubes are compared, it is found that the CFE and SEA of empty GFRP tube is 83% and 59% larger than empty Al tubes, respectively.
- when the crashworthiness performances of empty Al and empty hybrid tubes are compared, it is found that

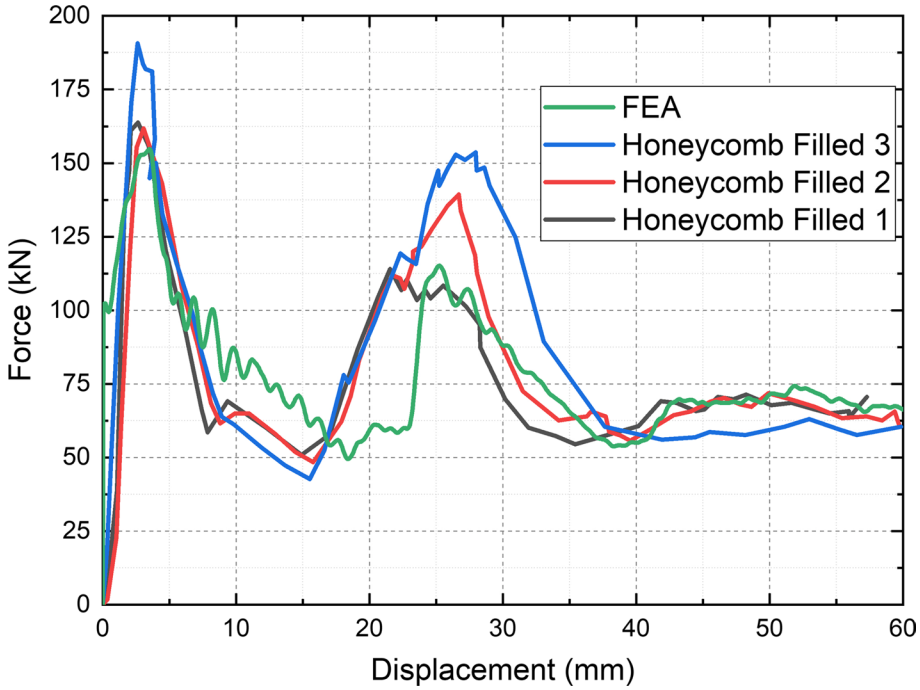

Fig. 21 Crushing load–displacement curves for honeycomb filled hybrid tubes

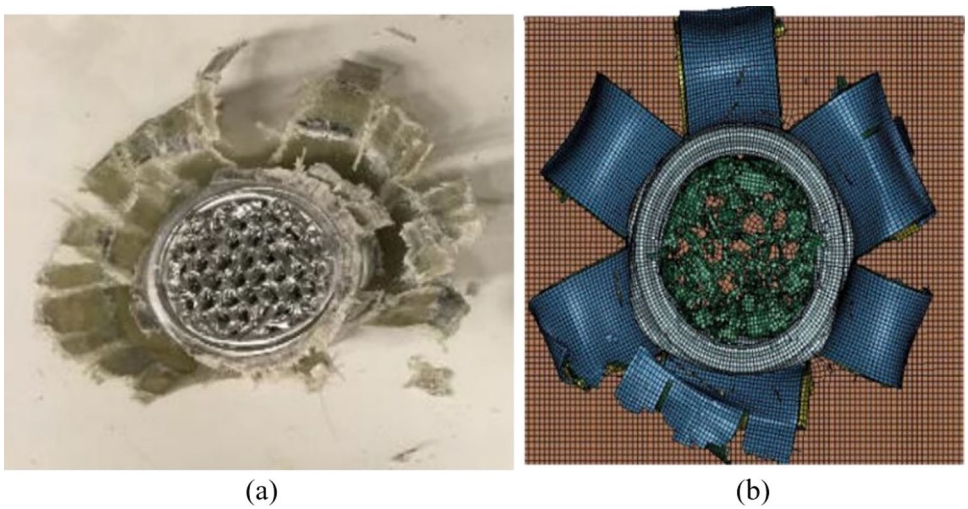

Fig. 22 Deformed view at 60 mm of deformation of honeycomb filled hybrid tubes: **a** experiment **b** FEA

Table 9 Comparison of energy absorption values between simulation and experimental results of honeycomb filled hybrid tubes

	Peak force (kN)	Mean force (kN)	CFE	EA (kJ)	Mass (kg)	SEA (kJ/kg)
Test	171.14	77.88	0.46	4.673	0.238	19.63
FEA	154.76	79.30	0.51	4.758	0.243	19.58
Error (%)	− 9.6	1.8	10.9	1.8	2.1	− 0.3

the CFE of the empty hybrid tube is 6% lower than the empty Al tube. However, SEA of empty hybrid tube is 23% larger than empty Al tube.

- when the crashworthiness performances of empty composite and empty hybrid tubes are compared, it is found that the CFE and SEA of the composite tube are 95% and 29% larger than the empty hybrid tube, respectively.
- when the crashworthiness performances of empty Al and honeycomb filled hybrid tubes are compared, it is found that the CFE of the empty hybrid tube is 2% lower than

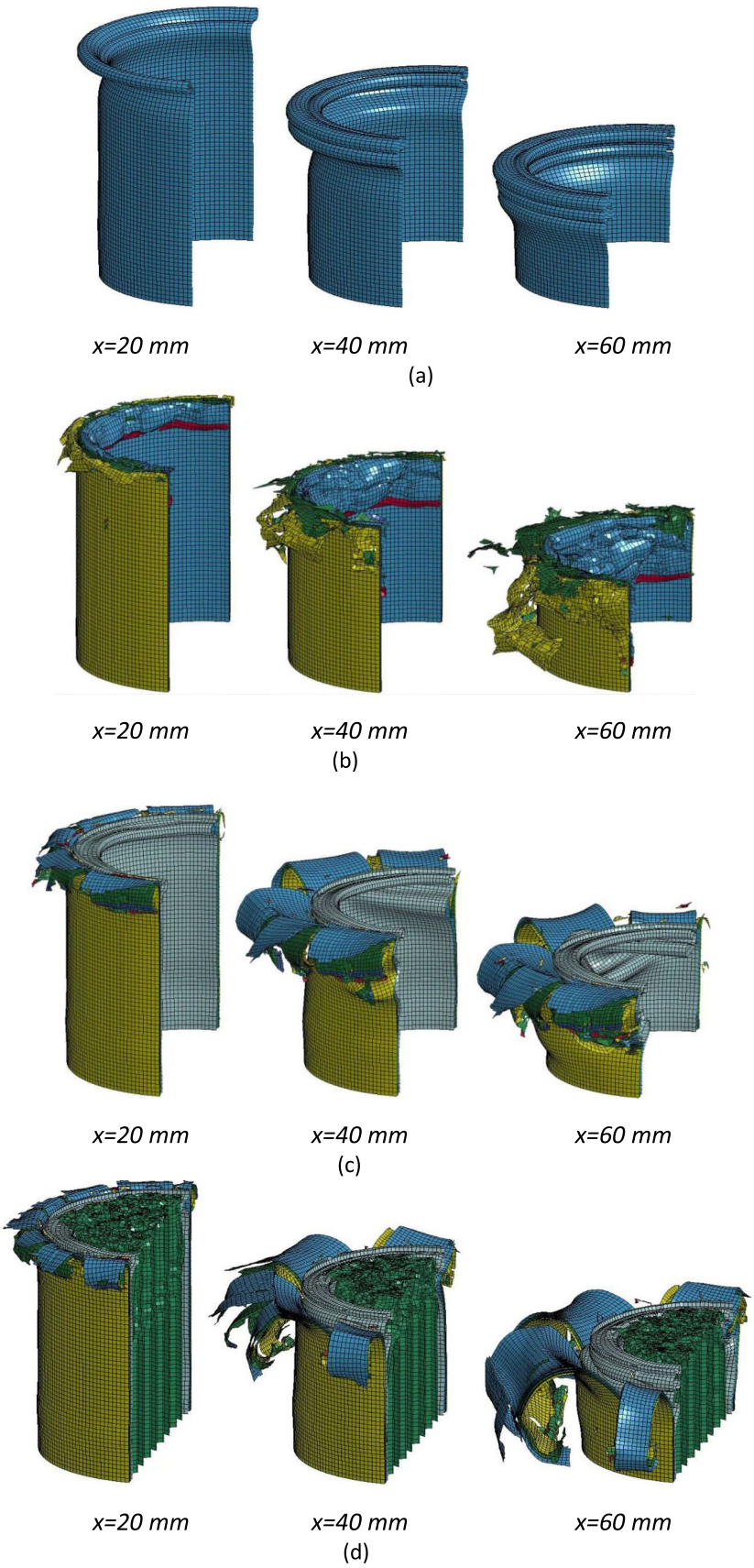

Fig. 23 Deformation views at 20 mm, 40 mm, and 60 mm of deformation of tubes: **a** aluminum tubes **b** GFRP tubes **c** hybrid tubes **d** honeycomb filled hybrid tubes

the empty Al tube. However, SEA of honeycomb filled hybrid tube is 6% larger than the empty Al tube.

- when the crashworthiness performances of empty and honeycomb filled hybrid tubes are compared, it is found that the CFE of the honeycomb filled hybrid tube is 4.5% larger than the empty hybrid tube. However, the SEA of honeycomb filled hybrid tube is 13% smaller than the empty hybrid tube.
- overall, the best performance in terms of both CFE and SEA was found to be in empty GFRP composite tubes. This might be attributed to the lower mass and density of GFRP composites.
- by applying a tuned trigger mechanism in the composite tubes, it is possible to get FEA results closely resembling the deformation process during the crushing of the tubes.

Acknowledgements The authors acknowledge the financial support provided by Ankara Yıldırım Beyazıt University, Department of Scientific Research Projects under Project No: 5582. The authors would like to express their gratitude to Hexagon Space Aviation Trade Ltd. for providing honeycomb aluminum fillers and Prof. Dr. Metin Tanoğlu and Murat Aydın for their contribution to characterization tests. Also, we would like to express our gratitude to Ameen Topa for his valuable, constructive criticisms during the modeling.

Declarations

Conflict of interest The authors declare that they have no conflict of interest.

References

1. Nikkhah H, Crupi V, Baroutaji A (2020) Crashworthiness analysis of bio-inspired thin-walled tubes based on Morpho wings microstructures. Mech Based Des Struct Mach 66:1–18
2. Malekshahi A, Hosseini M, Ansari AN (2020) Theoretical estimation of axial crushing behavior of multicell hollow sections. Mech Based Des Struct Mach 66:1–25
3. Fragoso-Medina O, Velázquez-Villegas F (2021) Aluminum foam to improve crash safety performance: a numerical simulation approach for the automotive industry. Mech Based Des Struct Mach 66:1–15
4. Altin M, Acar E, Güler M (2018) Foam filling options for crashworthiness optimization of thin-walled multi-tubular circular columns. Thin-Walled Struct 131:309
5. Acar E, Altin M, Güler MA (2019) Evaluation of various multicell design concepts for crashworthiness design of thin-walled aluminum tubes. Thin-Walled Struct 142:227
6. Mert SK, Demiral M, Altin M, Acar E, Güler MA (2021) Experimental and numerical investigation on the crashworthiness optimization of thin-walled aluminum tubes considering damage criteria. J Braz Soc Mech Sci Eng 43(2):1
7. Albak Eİ, Solmaz E, Yıldız AR, Öztürk F (2021) Multiobjective crashworthiness optimization of graphene type multi-cell tubes under various loading conditions. J Braz Soc Mech Sci Eng 43(5):1
8. Khorasani A, Saeidi Googarchin H (2021) Theoretical development and numerical analysis on the energy absorption of tapered multi-cell automotive structures under oblique impacts. Mech Based Des Struct Mach 66:1–19
9. Aktaş C, Acar E, Güler MA, Altın M (2022) An investigation of the crashworthiness performance and optimization of tetra-chiral and reentrant crash boxes. Mech Based Des Struct Mach 66:1–24
10. Ma X, Tian X (2022) Crushing behaviour of a novel hybrid multicell structure. J Braz Soc Mech Sci Eng 44(9):1
11. Alkhatib F, Mahdi E, Dean A (2020) Crushing response of CFRP and KFRP composite corrugated tubes to quasi-static slipping axial loading: experimental investigation and numerical simulation. Compos Struct 246:112370
12. Kumar AP, Shunmugasundaram M, Sivasankar S, Sankar LP (2020) Static axial crushing response on the energy absorption capability of hybrid Kenaf/Glass fabric cylindrical tubes. Mater Today Proc 27:783
13. Bakar MSA, Salit MS, Yusoff MZM, Zainudin ES, Ya HH (2020) The crashworthiness performance of stacking sequence on filament wound hybrid composite energy absorption tube subjected to quasi-static compression load. J Mater Res Technol 9(1):654
14. Xu J, Ma Y, Zhang Q, Sugahara T, Yang Y, Hamada H (2016) Crashworthiness of carbon fiber hybrid composite tubes molded by filament winding. Compos Struct 139:130
15. Özbek Ö, Doğan NF, Bozkurt ÖY (2020) An experimental investigation on lateral crushing response of glass/carbon intraply hybrid filament wound composite pipes. J Braz Soc Mech Sci Eng 42(7):1
16. Huang J, Wang X (2010) On a new crush trigger for energy absorption of composite tubes. Int J Crashworthiness 15(6):625
17. Chiu LN, Falzon BG, Ruan D, Xu S, Thomson RS, Chen B, Yan W (2015) Crush responses of composite cylinder under quasi-static and dynamic loading. Compos Struct 131:90
18. de Oliveira SAC, Donadon MV, Arbelo MA (2020) Crushing simulation using an energy-based damage model. J Braz Soc Mech Sci Eng 42(6):1
19. Taghipoor H, Eyvazian A (2022) Quasi-static axial crush response and energy absorption of composite wrapped metallic thin-walled tube. J Braz Soc Mech Sci Eng 44(4):1
20. Sun G, Chen D, Zhu G, Li Q (2022) Lightweight hybrid materials and structures for energy absorption: a state-of-the-art review and outlook. Thin-Walled Struct 172:108760
21. Isaac CW, Ezekwem C (2021) A review of the crashworthiness performance of energy absorbing composite structure within the context of materials, manufacturing and maintenance for sustainability. Compos Struct 257:113081
22. Wang L, Fan X, Chen H, Liu W (2016) Axial crush behavior and energy absorption capability of foam-filled GFRP tubes under elevated and high temperatures. Compos Struct 149:339
23. Palanivelu S, Van Paepegem W, Degrieck J, Vantomme J, Kakogiannis D, Van Ackeren J, Van Hemelrijck D, Wastiels J (2011) Crushing and energy absorption performance of different geometrical shapes of small-scale glass/polyester composite tubes under quasi-static loading conditions. Compos Struct 93(2):992
24. Özbek Ö, Bozkurt ÖY, Erkliğ A (2022) Development of a trigger mechanism with circular cut-outs to improve crashworthiness characteristics of glass fiber-reinforced composite pipes. J Braz Soc Mech Sci Eng 44(1):1
25. Chen D, Liu Y, Meng M, Li B, Sun X, Yang B, Xiao S, Wang T (2023) Dynamic axial crushing behaviors of circular composite tubes with different reinforcing fibers and triggers. Int J Mech Sci 244:108083
26. Awdallah MM, Abd El-baky MA, Hassan MA, Shaker A (2022) Crashworthiness performance of thin-walled glass/epoxy square tubes with circular cutouts: an experimental study. Fibers Polym 23(11):3268
27. Wang L, Liu W, Fang Y, Wan L, Huo R (2016) Axial crush behavior and energy absorption capability of foam-filled GFRP

tubes manufactured through vacuum assisted resin infusion process. Thin-Walled Struct 98:263
28. Othman A, Abdullah S, Ariffin A, Mohamed N (2016) Investigating the crushing behavior of quasi-static oblique loading on polymeric foam filled pultruded composite square tubes. Compos Part B Eng 95:493
29. Chen L, Pan D, Zhao Q, Niu L, Cong L, Li C (2021) Overall buckling characteristics of slender FRP-foam sandwich tube under axial compression. Compos Commun 24:100585
30. Jin Q, Wang J, Chen J, Bao F (2022) Axial compressive behavior and energy absorption of syntactic foam-filled GFRP tubes with lattice frame reinforcement. Compos Struct 299:116080
31. Wang J, GangaRao H, Li M, Liang R, Liu W (2019) Axial behavior of columns with glass fiber-reinforced polymer composite shells and syntactic foam core. J Compos Constr 23(2):04018083
32. Sarkhosh R, Farrokhabadi A, Zarei H (2022) Crashworthiness characteristics of composite cylindrical energy absorbers filled with honeycomb and foam under quasi-static load: experimental and analytical study. J Braz Soc Mech Sci Eng 44(8):346
33. Jiang H, Liu X, Jiang S, Ren Y (2023) Hybrid effects and interactive failure mechanisms of hybrid fiber composites under flexural loading: carbon/Kevlar, carbon/glass, carbon/glass/Kevlar. Aerosp Sci Technol 66:108105
34. Mirzaei M, Shakeri M, Sadighi M, Akbarshahi H (2012) Experimental and analytical assessment of axial crushing of circular hybrid tubes under quasi-static load. Compos Struct 94(6):1959
35. Song HW, Wan ZM, Xie ZM, Du XW (2000) Axial impact behavior and energy absorption efficiency of composite wrapped metal tubes. Int J Impact Eng 24(4):385
36. Shin KC, Lee JJ, Kim KH, Song MC, Huh JS (2002) Axial crush and bending collapse of an aluminum/GFRP hybrid square tube and its energy absorption capability. Compos Struct 57(1–4):279
37. Tarafdar A, Liaghat G, Ahmadi H, Razmkhah O, Charandabi SC, Faraz MR, Pedram E (2021) Quasi-static and low-velocity impact behavior of the bio-inspired hybrid Al/GFRP sandwich tube with hierarchical core: experimental and Numerical Investigation. Compos Struct 276:114567
38. Babbage J, Mallick P (2005) Static axial crush performance of unfilled and foam-filled aluminum-composite hybrid tubes. Compos Struct 70(2):177
39. Guden M, Yüksel S, Taşdemirci A, Tanoğlu M (2007) Effect of aluminum closed-cell foam filling on the quasi-static axial crush performance of glass fiber reinforced polyester composite and aluminum/composite hybrid tubes. Compos Struct 81(4):480
40. Subbaramaiah R, Prusty B, Pearce G, Lim S, Thomson R (2017) Crashworthy response of fibre metal laminate top hat structures. Compos Struct 160:773
41. El-Hage H, Mallick P, Zamani N (2006) A numerical study on the quasi-static axial crush characteristics of square aluminum-composite hybrid tubes. Compos Struct 73(4):505
42. Han H, Taheri F, Pegg N, Lu Y (2007) A numerical study on the axial crushing response of hybrid pultruded and ±45 braided tubes. Compos Struct 80(2):253
43. Zhang Z, Sun W, Zhao Y, Hou S (2018) Crashworthiness of different composite tubes by experiments and simulations. Compos Part B Eng 143:86
44. Farokhi Nejad A, Koloor SSR, Arifin MLH, Shafiei A, Hassan SA, Yahya MY (2022) Crashworthiness assessment of carbon/glass epoxy hybrid composite tubes subjected to axial loads. Polymers 14(19):4083
45. Mansor M, Ahmad Z, Abdullah M (2022) Crashworthiness capability of thin-walled fibre metal laminate tubes under axial crushing. Eng Struct 252:113660
46. Mamalis A, Manolakos D, Demosthenous G, Ioannidis M (1997) The static and dynamic axial crumbling of thin-walled fibreglass composite square tubes. Compos Part B Eng 28(4):439
47. Hussein RD, Ruan D, Lu G (2018) An analytical model of square CFRP tubes subjected to axial compression. Compos Sci Technol 168:170
48. Mamalis A, Manolakos D, Demosthenous G, Ioannidis M (1996) Analysis of failure mechanisms observed in axial collapse of thin-walled circular fibreglass composite tubes. Thin-Walled Struct 24(4):335
49. Solaimurugan S, Velmurugan R (2007) Progressive crushing of stitched glass/polyester composite cylindrical shells. Compos Sci Technol 67(3–4):422
50. Boria S, Pettinari S, Giannoni F (2013) Theoretical analysis on the collapse mechanisms of thin-walled composite tubes. Compos Struct 103:43
51. Mamalis A, Manolakos D, Demosthenous G, Ioannidis M (1997) Analytical modelling of the static and dynamic axial collapse of thin-walled fibreglass composite conical shells. Int J Impact Eng 19(5–6):477
52. Gupta N, Velmurugany R (2002) Experiments and analysis of collapse behaviour of composite domes under axial compression. J Compos Mater 36(8):899
53. Wierzbicki T et al (1996) Axial resistance and energy absorption of externally reinforced metal tubes. Compos Part B Eng 27(5):387
54. Wang X, Lu G (2002) Axial crushing force of externally fibre-reinforced metal tubes. Proc Inst Mech Eng Part C J Mech Eng Sci 216(9):863
55. Siromani D, Awerbuch J, Tan TM (2014) Finite element modeling of the crushing behavior of thin-walled CFRP tubes under axial compression. Compos Part B Eng 64:50
56. Rabiee A, Ghasemnejad H (2022) Finite element modelling approach for progressive crushing of composite tubular absorbers in LS-DYNA: review and findings. J Compos Sci 6(1):11
57. Huang J, Wang X (2009) Numerical and experimental investigations on the axial crushing response of composite tubes. Compos Struct 91(2):222
58. Rabiee A, Ghasemnejad H (2016) Effect of multi stitched locations on high speed crushing of composite tubular structures. Compos Part B Eng 100:164
59. Atthapreyangkul A, Prusty BG (2017) Experimental and numerical analysis on the geometrical parameters towards the maximum SEA of CFRP components. Compos Struct 164:229
60. Tong Y, Xu Y (2018) Improvement of crash energy absorption of 2D braided composite tubes through an innovative chamfer external triggers. Int J Impact Eng 111:11
61. Boria S, Obradovic J, Belingardi G (2015) Experimental and numerical investigations of the impact behaviour of composite frontal crash structures. Compos Part B Eng 79:20
62. Boria S, Pettinari S, Giannoni F, Cosimi G (2016) Analytical and numerical analysis of composite impact attenuators. Compos Struct 156:348
63. Reuter C, Sauerland KH, Tröster T (2017) Experimental and numerical crushing analysis of circular CFRP tubes under axial impact loading. Compos Struct 174:33
64. Meriç D, Gedikli H (2022) Multi-objective optimization of energy absorbing behavior of foam-filled hybrid composite tubes. Compos Struct 279:114771
65. Ls-Dyna LD (2016) Keyword users manual-volume II: material models. Livermore Software Technology Corporation, Livermore
66. Yibo P, Gang W, Tianxing Z, Shangfeng P, Yiming R (2013) Dynamic mechanical behaviors of 6082-T6 aluminum alloy. Adv Mech Eng 5:878016

67. Chen D, Xiao S, Yang B, Yang G, Zhu T, Wang M, Zhang Z (2022) Axial crushing response of carbon/glass hybrid composite tubes: an experimental and multi-scale computational study. Compos Struct 66:115640